Thermodynamics of plasmaballs and plasmarings in 3+1 dimensions

JHEP03(2009)101

(http://iopscience.iop.org/1126-6708/2009/03/101)

Published by IOP Publishing for SISSA

Received: *January 19, 2009*
Accepted: *February 22, 2009*
Published: *March 17, 2009*

Thermodynamics of plasmaballs and plasmarings in 3+1 dimensions

Shanthanu Bhardwaj[a] **and Jyotirmoy Bhattacharya**[b]

[a] *Department of Physics, University of Chicago, Chicago, IL 60637-1434, U.S.A.*
[b] *Department of Theoretical Physics, Tata Institute of Fundamental Research, Homi Bhabha Rd, Mumbai 400005, India*

E-mail: shanth@uchicago.edu, jyotirmoy@theory.tifr.res.in

Abstract: We study localized plasma configurations in $3+1$ dimensional massive field theories obtained by Scherk-Schwarz compactification of $4+1$ dimensional CFT to predict the thermodynamic properties of localized blackholes and blackrings in Scherk-Schwarz compactified AdS_6 using the AdS/CFT correspondence. We present an exact solution to the relativistic Navier-Stokes equation in the thin ring limit of the fluid configuration. We also perform a thorough numerical analysis to obtain the thermodynamic properties of the most general solution. Finally we compare our results with the recent proposal for the phase diagram of blackholes in six flat dimensions and find some similarities but other differences.

Keywords: Gauge-gravity correspondence, AdS-CFT Correspondence, Black Holes

ArXiv ePrint: 0806.1897

doi:10.1088/1126-6708/2009/03/101

JHEP03(2009)101

Contents

JHEP03(2009)101

1 Introduction

Black holes in dimensions greater than four have recently drawn considerable interest [1–3]. They not only provide testing ground of String theory (for example counting of microstates to obtain the entropy) but also are interesting in their own right as they aid the greater understanding of General Relativity. In this note we use the AdS/CFT correspondence to study black holes in six dimensional space-times that asymptote to a Scherk-Schwarz compactification of AdS_6. Although it appears to be difficult to directly construct black hole backgrounds in these geometries, the AdS/CFT correspondence identifies finite energy configurations of the 'deconfined gluon plasma' fluid of the dual boundary field theory with these localized black holes permitting a detailed study of the spectrum of black holes and their thermodynamic properties in appropriate limits [4].

In more detail, the dual boundary description of gravity on a background that asymptotes to a Scherk-Schwarz compactification of AdS_6 is given by the Scherk-Schwarz compactification of a $4+1$ dimensional CFT. The effective long distance description of this system is given by the $3+1$ fluid dynamics equations (the relativistic Navier-Stokes equations) with the appropriate equation of state and dissipative parameters, all of which are

directly known from gravity. In an appropriate limit, rotating bulk black holes are dual to localized rotating lumps of the boundary fluid that solve the Navier-Stokes equations. Such fluid configurations were investigated in [5] (see [6] for a prior discussion on equilibrium fluid configurations and analysis of their stability in relation to the study of black holes). The authors of [5] constructed solutions of fluid dynamics with the topology of a ball and other solutions with the topology of a solid torus. They argued that, under the AdS/CFT correspondence described above, these solutions are dual to black objects whose horizons are topologically S^4 and $S^3 \otimes S^1$ respectively, i.e. black holes and black rings.

The authors of [5], however, left open the possibility of the existence of other topologically distinct solutions of fluid dynamics which would be dual to black holes with distinct horizon topologies. They also did not study the thermodynamic properties of the solutions they have constructed. Finally, the solutions of [5], while explicit, are presented in terms of a function defined by a definite integral that appears difficult to control analytically.

In this paper we continue (and to an extent complete) the analysis of [5] in three different ways. First we perform a thorough numerical scan to demonstrate that the rotating fluid solutions presented in [5] are the only stationary rotating solutions of the relevant Navier-Stokes equations. Second we determine the thermodynamic properties and the phase diagram of the solutions constructed in [5]. Finally we also find a particular limit (the 'thin ring' limit) in which the integrals of [5] may be explicitly evaluated. All thermodynamic properties may be evaluated analytically in this limit, allowing a better intuitive understanding of the properties of these solutions, and providing checks on our (numerical) determination of the thermodynamic properties of the general solution.

The thermodynamic properties of the ball and ring solutions of [5] turn out to be very similar to the properties of the analogous solutions in one lower dimension (discussed in detail in [5]). In figure 1 we present a plot of the entropy versus the angular momentum of the relevant solutions, at a fixed value of the energy. As is apparent from figure 1 we find at least one rotating fluid solution for every value of the angular momentum. However in a particular window of angular momentum - in the range (L_B, L_C) - there exist three solutions which have the same energy and angular momentum. These three solutions may be thought of as a ball a thick ring and a thin ring respectively of rotating fluid. The ball solution is entropically dominant for $L < L_P$ while the thin ring dominates for $L > L_P$. At angular momentum L_P (which lies in the range (L_B, L_C)) the system (in the microcanonical ensemble) consequently undergoes a 'first order phase transition' from the ball to the ring. It follows that the dual gravitational system must exhibit a dual phase transition from a black hole to a black ring at the same angular mumomentum.

In section 6 we explain that the phase diagram depicted in figure 1 has some similarities, but several qualitative points of difference from a conjectured phase diagram for the solution space of rotating black holes and black rings in 6 dimensional flat spacetime. This suggests that the properties of black holes and black rings in 6 dimensional AdS space are rather different from those of the corresponding objects in flat six dimensional space. This is a bit of a surprise, as black holes and rings in Scherk-Schwarz compactified AdS_5 appear to have properties that are qualitatively similar to their flat space counterparts [3, 5]. The rest of this paper is organized as follows. In section 2 below we review the results of [5]. In section 3

JHEP03(2009)101

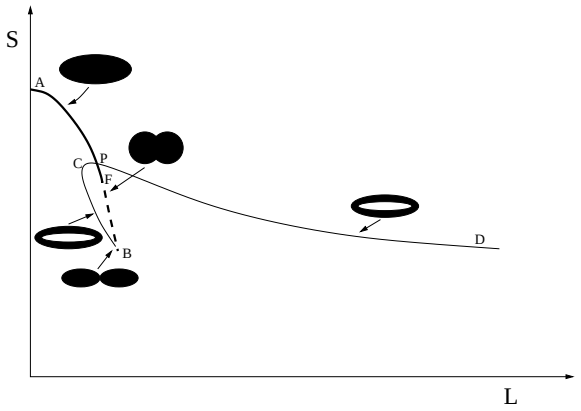

Figure 1. Schematic plot of the phase diagram for the various plasma configurations which by AdS/CFT correspondence gives the phase structure of blackholes with various horizon topologies in Scherk-Schwarz compactified AdS_6.

we describe the numerical scan that has convinced us that there exist no further solutions to the equations of [5] in addition to the ball and ring solutions presented in that paper. In section 4 we analytically determine the ring solution and its thermodynamic properties in the 'thin ring' limit. We also study the properties of the ball and ring solutions at the point in moduli space where they meet; the point at which the ball just squeeze off into a ring. In section 5 we present a thorough numerical analysis of the thermodynamic properties of the ball and ring solutions, and the resultant phase diagram of the system. in section 6 we compare this phase diagram to the conjectured phase diagram for spinning black holes and black rings in flat space, presented by Emparan and collaborators [1].

2 Review

Here we briefly summarize the results of [5] as we intend to study the thermodynamic properties of the solutions already presented there. We also borrow our notations and conventions from therein. For the study of $3+1$ dimensional plasma configurations we work with the coordinates (t, r, ϕ, z) and the metric we consider is,

$$ds^2 = -dt^2 + dr^2 + r^2 d\phi^2 + dz^2. \tag{2.1}$$

Considering the axis of rotation (whenever applicable) to be the z-axis we assume that the surface of the plasma configuration is given by the surface $z - h(r) = 0$, with $h(r)$ being a height function. The equation of state for the fluid under consideration is,

$$F = V\left(\rho_0 - \lambda \mathcal{T}^5\right), \tag{2.2}$$

where F and $\mathcal{T}$ are the free energy and temperature respectively, ρ_0 denotes the vacuum energy density and λ being some arbitrary constant (note that λ here is *not* 't Hooft coupling). In terms of the intensive variables the equation of state can be written as,

$$P = \frac{\rho - 5\rho_0}{4}, \quad s = 5\lambda^{\frac{1}{5}}\left(\frac{\rho - \rho_0}{4}\right)^{\frac{4}{5}}, \tag{2.3}$$

JHEP03(2009)101

where P, s and ρ are respectively the pressure, entropy density and energy density.

We now consider the energy momentum tensor as worked out in [5]. In a frame where the four velocity is $u^\mu = \gamma(1, 0, \omega, 0)$, the perfect fluid stress tensor and the surface stress tensor are respectively given by,

$$T^{\mu\nu}_{\text{perfect}} = \begin{pmatrix} \gamma^2\left(Pr^2\omega^2+\rho\right) & 0 & \omega\gamma^2(P+\rho) & 0 \\ 0 & P & 0 & 0 \\ \omega\gamma^2(P+\rho) & 0 & \frac{\gamma^2\left(Pr^2\omega^2+\rho\right)}{r^2} & 0 \\ 0 & 0 & 0 & P \end{pmatrix} \tag{2.4}$$

$$T^{\mu\nu}_{\text{surface}} = \frac{\delta(z-h(r))\sigma}{\sqrt{h'(r)^2+1}} \begin{pmatrix} h'(r)^2+1 & 0 & 0 & 0 \\ 0 & -1 & 0 & -h'(r) \\ 0 & 0 & -\frac{h'(r)^2+1}{r^2} & 0 \\ 0 & -h'(r) & 0 & -h(r)^2 \end{pmatrix} \tag{2.5}$$

where $\gamma = (1-\omega^2 r^2)^{-\frac{1}{2}}$, P is the local pressure of the fluid configuration and σ is the surface tension . The hydrodynamic equations given by $\nabla_\mu T^{\mu\nu} = 0$ reduces to,

$$\frac{\partial P}{\partial r} - \frac{\omega^2 r(\rho+P)}{\sqrt{1-\omega^2 r^2}} \mp 2\sigma H h'(r)\delta(z-h(r)) = 0, \tag{2.6}$$

$$\frac{\partial P}{\partial z} \pm 2\sigma H \delta(z-h(r)) = 0. \tag{2.7}$$

where,

$$H = \mp \frac{h'(r)\left(h'(r)^2+1\right) + rh''(r)}{2r\left(h'(r)^2+1\right)^{3/2}} \tag{2.8}$$

the upper sign referring to the upper($z > 0$) surface.

We do not consider the dissipative terms in the stress tensor because we are interested in non-dissipative solutions. The dissipative part of the stress tensor vanishes on the solutions constructed in [5] (those that are considered by us in this paper).

We define certain dimensionless variables as follows,

$$\tilde{\omega} = \frac{\sigma\omega}{\rho_0}, \quad v = \omega r, \quad \tilde{h}(v) = \omega h(r), \tag{2.9}$$

where ω is the angular velocity of the fluid configuration.

Now integrating (2.6) and (2.7) in the bulk interior away from the outer or inner surface (and also using the equation of state (2.3)) we have,

$$P = \rho_0 \left(\frac{k}{(1-v^2)^{\frac{5}{2}}} - 1 \right) \tag{2.10}$$

where k is an integration constant depending on the bulk properties of the plasma fluid.

Again integrating (2.7) across an outer surface gives,

$$P = 2\sigma H \tag{2.11}$$

JHEP03(2009)101

For convenience we define two functions,

$$f(v) = 2k - 3\left(v^2 + 2c\right)\left(1 - v^2\right)^{\frac{3}{2}}, \quad g(v) = 6\tilde{\omega}v\left(1 - v^2\right)^{\frac{3}{2}}. \tag{2.12}$$

Now using (2.10) and (2.8) into (2.11) we obtain a second order differential equation for the height function $\tilde{h}(v)$. This equation can be integrated once to obtain,

$$\frac{d\tilde{h}}{dv} = \frac{-f(v)}{(g(v)^2 - f(v)^2)^{\frac{1}{2}}}, \tag{2.13}$$

which on further integration yields,

$$\tilde{h}(v) = \int_{v_o}^{v} \frac{-f(x)}{(g(x)^2 - f(x)^2)^{\frac{1}{2}}} dx. \tag{2.14}$$

Here c is another constant determined by the surface properties of the fluid.

If there is an inner surface of the plasma configuration then it is also obtained by the same procedure, but this time we have the opposite sign,

$$P = -2\sigma H \tag{2.15}$$

Again integrating (2.15) we obtain the height function of an inner surface, which is given by,

$$\frac{d\tilde{h}}{dv} = \frac{f(v)}{(g(v)^2 - f(v)^2)^{\frac{1}{2}}}. \tag{2.16}$$

Now let us consider the various stationary solutions presented in [5] one by one.

1. *BALL*: This is obtained when the derivative of the height function is 0 at $v = 0$ and $-\infty$ at the outer radius $v = v_o$ and the height function is monotonic in this interval of interest. The first condition implies $k = 3c$, the second implies $f(v_o) = g(v_o)$ and the third implies k must always be greater than 1. We also compute the expressions for energy, angular momentum and entropy. Energy (obtained from the time-time component of the energy momentum tensor) is given by,

$$E = \frac{4\pi\sigma^3}{\rho_0^2\tilde{\omega}} \int_0^{v_o} dv \left(\tilde{h}(v)v \left(\frac{k\left(4 + v^2\right)}{\left(1 - v^2\right)^{\frac{7}{2}}} + 1 \right) + \tilde{\omega}v \left(1 + \tilde{h}'(v)^2\right)^{\frac{1}{2}} \right). \tag{2.17}$$

   Angular momentum is obtained from the $t\phi$ component of the energy momentum tensor and is given by,

$$L = \frac{20\pi k\sigma^4}{\rho_0^3\tilde{\omega}^4} \int_0^{v_o} \frac{v^3\tilde{h}(v)dv}{\left(1 - v^2\right)^{\frac{7}{2}}}. \tag{2.18}$$

   Finally the Entropy is obtained from the expression of entropy density as in (2.3) and is given by,

$$S = \frac{20\pi\lambda^{\frac{1}{5}}k^{\frac{4}{5}}\sigma^3}{\rho_0^{\frac{11}{5}}\tilde{\omega}^3} \int_0^{v_o} \frac{v\tilde{h}(v)dv}{\left(1 - v^2\right)^{\frac{5}{2}}}. \tag{2.19}$$

JHEP03(2009)101

2. *PINCHED BALL*: This solution is topologically same as the ball. So the conditions on the derivative of the height function is same as in the case of the ball. However the important difference here is that the height function is not monotonic. This allows for values of k less than 1 only. The reality condition for the height function demands k to be greater than 0. Further restriction on the parameter space is provided by the fact that the height function at $v = 0$ cannot exceed that at $v = v_o$ (where it is 0). In other words $\tilde{h}(0)$ must be greater than $\tilde{h}(v_o) = 0$. This condition may be stated as follows,

$$\Delta\tilde{h} = \int_0^{v_0} \frac{-f(x)dx}{(g(v)^2 - f(v)^2)^{\frac{1}{2}}} \geq 0. \tag{2.20}$$

The expressions for energy, angular momentum and entropy is exactly the same as in the case of the ball solution, the only difference being that here we are dealing with a different region of parameter space.

3. *RING*: In the case of the ring $\tilde{h}'(v)$ must be ∞ and $-\infty$ respectively at the inner and outer radius v_i and v_o (rigorously these are the velocities at the inner and outer radius of the ring). This sets the following conditions,

$$\begin{aligned} f(v_o) &= g(v_o), \\ f(v_i) &= -g(v_i). \end{aligned} \tag{2.21}$$

Further the condition that $\tilde{h}(v)$ at both ends v_i and v_o should be equal (both being equal to 0), sets the following condition,

$$\Delta\tilde{h} = \int_{v_i}^{v_0} \frac{-f(v)dv}{(g(v)^2 - f(v)^2)^{\frac{1}{2}}} = 0. \tag{2.22}$$

In the expressions for energy, angular momentum and entropy the lower limit of the integral gets modified for the ring and we have,

$$\begin{aligned} E &= \frac{4\pi\sigma^3}{\rho_0^2\tilde{\omega}} \int_{v_i}^{v_o} dv \left(\tilde{h}(v)v \left(\frac{k\left(4+v^2\right)}{(1-v^2)^{\frac{7}{2}}} + 1 \right) + \tilde{\omega}v \left(1 + \tilde{h}'(v)^2\right)^{\frac{1}{2}} \right), \\ L &= \frac{20\pi k\sigma^4}{\rho_0^3\tilde{\omega}^4} \int_{v_i}^{v_o} \frac{v^3\tilde{h}(v)dv}{(1-v^2)^{\frac{7}{2}}}, \\ S &= \frac{20\pi\lambda^{\frac{1}{5}}k^{\frac{4}{5}}\sigma^3}{\rho_0^{\frac{11}{5}}\tilde{\omega}^3} \int_{v_i}^{v_o} \frac{v\tilde{h}(v)dv}{(1-v^2)^{\frac{5}{2}}}. \end{aligned} \tag{2.23}$$

For convenience we define the following dimensionless quantities,

$$\tilde{E} = \frac{\rho_0^2 E}{4\pi\sigma^3}, \quad \tilde{L} = \frac{\rho_0^3 L}{20\pi\sigma^4}, \quad \tilde{S} = \frac{\rho_0^{\frac{11}{5}} S}{20\pi\lambda^{\frac{1}{5}}\sigma^3}. \tag{2.24}$$

We shall use these quantities for our later analysis.

JHEP03(2009)101

3 Existence of other possible configurations

Besides the ball, pinched ball and the ring solutions discussed in section 2 we can have the following topologies for the plasma configuration

- Hollow ball - a ball with a ball scooped out from inside it.
- Hollow ring - a ring with a ring scooped out from within.
- Torridally hollow ball - a ball with a ring cut out from inside.

The existence of the Hollow ball was already ruled out in [5]. Thefore we consider the possibility of the existence of ring-like inner surface of a configuration.

If a ring is to exist as an inner surface then instead of (2.21), it should satisfy the following condition,

$$\begin{aligned} f(v_o) &= -g(v_o), \\ f(v_i) &= g(v_i). \end{aligned} \tag{3.1}$$

The condition (2.22) remains unchanged. We considered k, v_i and v_o as the parameters of the ring. Actually there should be two parameters. However the relation (2.22) could not be easily used to express k in terms of the other parameters. Then we numerically scanned the three dimensional parameter space from 0 to 1 in all directions (note that although 1 is not the upper limit of k, for the other two parameters it is). All the parameters were varied by an interval of 0.01. With these values of the parameters we evaluated $\Delta\tilde{h}$. We found (for $v_i \neq v_o$) $\Delta\tilde{h}$ was negative (except when v_i was very close to zero and v_o was very close to one-when the numerical computations were no longer reliable). This eliminates (up to numerical accuracies of the scan) the possibility of the existence of a ring like inner surface both inside a ball as well as a ring.

4 Analytical results

In this section we study the solutions presented in [5] in certain analytically tractable limits.

4.1 The thin ring limit

It was possible to obtain an analytical solution of the hydrodynamic equations in the thin ring limit (i.e. $(v_o - v_i)$ is very small) as we shall discuss in this subsection. Let us define the quantities,

$$a = \frac{v_o + v_i}{2}; \quad \alpha a = \frac{v_o - v_i}{2}. \tag{4.1}$$

It is sometimes convenient to choose a, α as the two parameters in the problem. The thin ring limit then corresponds to choosing α to be an infinitesimal parameter. In terms of a, α the equations (2.21) and (2.22) that constrained the parameter space of the ring solution

JHEP03(2009)101

may be written as,

$$f(a(1+\alpha)) = g(a(1+\alpha)), \tag{4.2}$$

$$f(a(1-\alpha)) = -g(a(1-\alpha)), \tag{4.3}$$

$$\int_{a(1+\alpha)}^{a(1-\alpha)} \frac{f(v)dv}{(g(v)^2 - f(v)^2)^{\frac{1}{2}}} = 0. \tag{4.4}$$

These three equations may be used to obtain $k, \tilde{\omega}, c$ in terms of a, α.

Now, in order to satisfy these equations, let us start with the ansatz:

$$f(a+x) = \frac{x}{a\alpha} g(a+x) \tag{4.5}$$

This form of $f(v)$, clearly satisfies the above conditions (4.2), (4.3), (4.4), and leads to the conditions:

$$f(a) = 0 \tag{4.6}$$

$$a\alpha f'(a) = g(a) \tag{4.7}$$

$$\frac{1}{2}(a\alpha) f''(a) = g'(a) \tag{4.8}$$

Similar conditions on the higher derivatives cannot be imposed since we have only 3 free parameters. To leading order in α these 3 parameters are determined to be,

$$\begin{aligned} k &= \frac{\left(1-a^2\right)^{\frac{7}{2}}}{1-6a^2} + O(\alpha), \\ \tilde{\omega} &= \frac{5a^3\alpha}{1-6a^2} + O(\alpha^2), \\ c &= \frac{20a^4 - 7a^2 + 2}{6(1-6a^2)} + O(\alpha). \end{aligned} \tag{4.9}$$

To estimate the errors in this calculation we must note that the first term in $f(a+x)$ that does not match correctly is the term $\frac{1}{2}g^{(2)}(a)\frac{x^3}{a\alpha}$. This term does not contribute to any change in the numerator of the integral, however, in the denominator it contributes a deviation of $O\left(x^3/\alpha\right)$, which lends to an error of $O\left(\alpha^2\right)$ overall.

Also under the small αa approximation the height function can be approximated as,

$$\begin{aligned} \tilde{h}(v) = \tilde{h}(x+a) = &\int_{-\alpha a}^{x} \frac{-f'(a)xdx}{\left(g(a)^2 - f'(a)^2x^2\right)^{\frac{1}{2}}} \\ =&\left(\alpha^2a^2 - (v-a)^2\right)^{\frac{1}{2}}, \end{aligned} \tag{4.10}$$

where we use $g(a) = (\alpha a)f'(a)$.

Now the angular momentum ($\tilde{L}$) energy ($\tilde{E}$) and entropy ($\tilde{S}$) in the small α limit is given by,

$$\tilde{L} = \frac{k}{\tilde{\omega}^4}\int_{v_i}^{v_o}\frac{v^3 h(v)dv}{(1-v^2)^{\frac{7}{2}}} \approx \frac{\sqrt{a^2}\left(1-6a^2\right)^3\pi}{1250a^8\alpha^2} \tag{4.11}$$

$$\tilde{S} = \frac{k^{\frac{4}{5}}}{\tilde{\omega}^3}\int_{v_i}^{v_o}\frac{vh(v)dv}{(1-v^2)^{\frac{5}{2}}} \approx -\frac{\sqrt{a^2}\left(1-6a^2\right)^2\left(a^2-1\right)\pi}{250a^7\sqrt[5]{-\frac{(1-a^2)^{7/2}}{6a^2-1}}\alpha(a)} \tag{4.12}$$

$$\tilde{E} = \frac{1}{\tilde{\omega}^3}\int_{v_i}^{v_o} dv\left(vh(v)\left(\frac{(4+v^2)k}{(1-v^2)^{\frac{7}{2}}}+1\right)+\frac{\tilde{\omega}va\alpha}{h(v)}\right) \approx \frac{\sqrt{a^2}\left(1-6a^2\right)^2\left(a^2+1\right)\pi}{50a^7\alpha} \tag{4.13}$$

The local temperature of the plasma is given by,

$$\mathcal{T} = \left(\frac{\rho-\rho_0}{4\lambda}\right)^{\frac{1}{5}} = \left(\frac{k\rho_0}{\lambda}\right)^{\frac{1}{5}}\gamma, \tag{4.14}$$

where $\gamma = \frac{1}{\sqrt{(1-v^2)}}$, v being the local velocity of the fluid.

Also the thermodynamic temperature of full plasma configuration is given by,

$$T = \left(\frac{\partial E}{\partial S}\right)_L = \left(\frac{\partial \tilde{E}}{\partial \tilde{S}}\right)_{\tilde{L}}\frac{1}{5}\left(\frac{\rho_0}{\lambda}\right)^{\frac{1}{5}}. \tag{4.15}$$

Now using relations (4.11), (4.12) and (4.13) we obtain the temperature to leading order in α as follows,

$$\frac{1}{T} = \beta = \left(\frac{\delta\tilde{S}}{\delta\tilde{E}}\right)_{\tilde{L}} = \frac{1}{5k^{\frac{1}{5}}} \tag{4.16}$$

so that temperature of the configuration is given by,

$$T = \mathcal{T}\sqrt{1-v^2}. \tag{4.17}$$

We can now use (4.13) to express α in terms of a and energy E,

$$\alpha = \frac{\sqrt{a^2}\left(1-6a^2\right)^2\left(a^2+1\right)\pi}{50a^7\tilde{E}} \tag{4.18}$$

Substituting α from (4.18) into (4.11) and (4.12) we are able to express $\tilde{L}$ and $\tilde{S}$ in terms of $\tilde{E}$ and a. Thus we can now fix $\tilde{E}$ and plot $\tilde{S}$ vs $\tilde{L}$ taking a to be a parameter. This plot is shown in figure 2 and in figure 3 for different values of energy.

4.1.1 Validity of the thin ring approximation

Our conclusions about the thin ring is valid only when we simultaneously meet the following conditions.

1. the thin ring limit is valid i.e. $\alpha \ll 1$
2. physical quantities like $\tilde{\omega}$ and $\tilde{L}$ are not negative.

JHEP03(2009)101

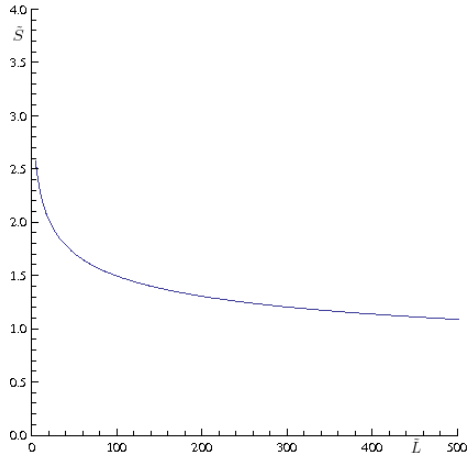

Figure 2. Here we plot entropy ($\tilde{S}$) against angular momentum ($\tilde{L}$) for $\tilde{E} = 10$ (note that even when the thin ring approximation is invalid for such low energies this plot agrees quite well with the numerical plots presented in section5.

3. we are within the domain of validity of hydrodynamics $\frac{\sigma}{\rho_0 R_c} \ll 1$. This physically means that the radius of the thin ring considered (R_c) is much larger than $\frac{\sigma}{\rho_0}$, the typical length scale at which the hydrodynamics assumption breaks down.

We now analyze the circumstances under which all of these conditions are simultaneously fulfilled. In the following discussion we parameterize our ring solution by its mean velocity a and its energy $\tilde{E}$.

The second condition listed above requires that $a \leq \frac{1}{\sqrt{6}}$ (see (4.9) (4.11)). The third condition — the validity of the fluid dynamical approximation — imposes the more stringent requirement $a \ll \frac{1}{\sqrt{11}}$. Finally the condition that $\alpha \ll 1$ is met provided

$$\frac{(1-6a^2)^2}{a^6\tilde{E}} \ll 1.$$

It follows that our analysis is valid in every respect only if $a \ll 1$ but $a^6\tilde{E} \gg 1$.

We conclude that the thin ring approximation described in this section is valid over a large region of parameter space provided that the energy $\tilde{E}$ is large. We illustrate this point in figure 3. In figure 3 we plot the entropy versus the angular momentum of the ring solutions at different values of $\tilde{E}$ using the thin ring formulas (4.11), (4.12), (4.13), and indicate the approximate region of validity of this approximation. As is apparent from this figure, the domain of validity of the thin ring approximation increases with increasing energy.

We note an intriguing property of the equations in the thin ring limit; they suggest a universal upper bound of $\frac{1}{\sqrt{6}}$ for the mean ring velocity. As a is taken to this upper bound value the thickness of the ring αa goes to zero. Unfortunately- as we have seen above - this phenomenon occurs outside the validity of the fluid dynamical approximation and so is not reliable. Nonetheless it is natural to wonder whether an exact version of this phenomenon is present for the true solutions of gravity.

JHEP03(2009)101

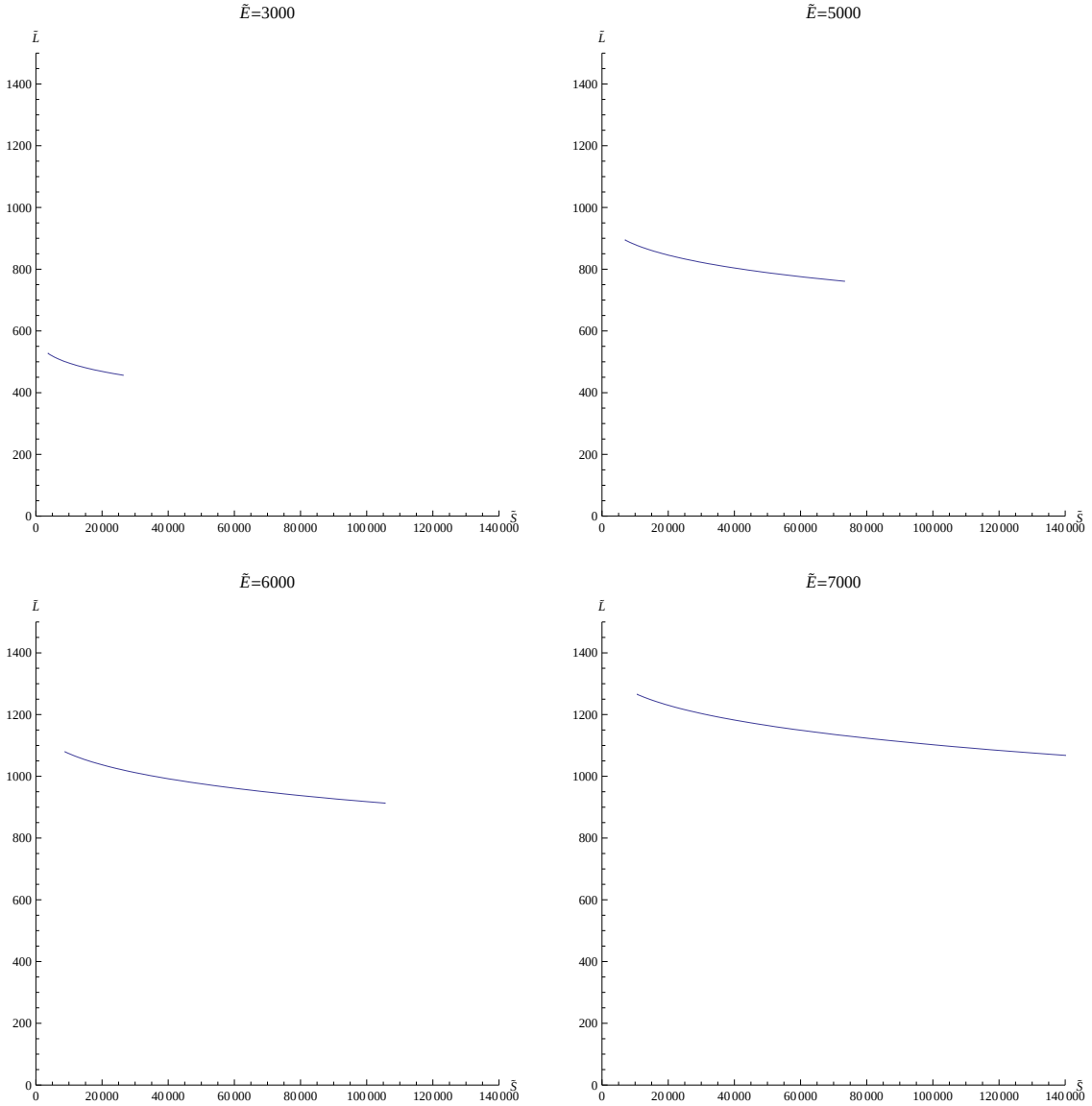

Figure 3. Here we again plot entropy ($\tilde{S}$) against angular momentum ($\tilde{L}$) for different fixed energies ($\tilde{E} = 3000, 5000, 6000, 7000$) within the domain of validity of the thin ring approximation. for all the plots the left end is the point where α is 0.1 and the right end is the point where the hydrodynamics assumption starts breaking down.

4.1.2 Physical interpretation

As we have seen in the previous subsection, the conclusions that follow from an analysis of the thin ring limit are valid - within the regime of fluid dynamics - only at small a. In this regime the fluid is approximately non relativistic, and all the formulas of the previous subsection may be derived in a much more elementary and physical fashion, as we will now explain.

In the thin ring limit we can think of the solution as a spinning narrow tube in the shape of a torus, parameterized by the two radius R_c (radius of the tube) and R (distance

JHEP03(2009)101

of the center of the tube from the center of the torus). We are now interested in the limit $\frac{R_c}{R} \to 0$. In this limit the plasmaring is a narrow tube that curves into a circle that is much larger than its thickness. As a consequence it is possible to focus on a segment of this ring that is large compared to R_c but small compared to R. To the zeroth approximation such a segment may be regarded as a cylinder of radius R_c. A simple force balance (surface tension versus pressure) on this cylinder tells us that the pressure of the fluid in this cylinder is given by

$$P = \frac{\sigma}{R_c} \tag{4.19}$$

Now the cylinder described above is not quite straight; it bends in the plane of the ring and also rotates in the same plane. Consequently, the condition for equilibrium at next order in an expansion of R_c/R require us to balance forces in the plane of the ring. This is also easily achieved. The centripetal acceleration of rotation, on any given segment of the ring, must be provided by the effective tension of the cylinder. This tension is given by $T = 2\pi R_c\sigma - \pi R_c^2 P = \pi R_c\sigma$. A force balance then yields $T = \pi R_c^2 R^2 \rho\omega^2$ so that

$$\omega^2 = \frac{\sigma}{\rho R_c R^2}, \tag{4.20}$$

Expressing this relation in terms of the quantities defined previously we obtain

$$\tilde{\omega} = \frac{5a^3\alpha}{1-4a^2} \approx 5a^3\alpha, \tag{4.21}$$

which agrees with (4.9) at leading order in a (we could not have expected our better agreement from our nonrelativistic arguments; see below however for the relativistic generalization). Now we are interested in the behavior of angular momentum L and entropy S keeping energy E fixed in the limit $R_c \to 0$. The energy expressed in terms of a and α up to leading order is (we do not include the surface contribution because it is not expected to contribute to the leading order),

$$E = \rho\left(2\pi R_c^2 R\right) + \frac{1}{2}\rho\left(2\pi R_c^2 R\right)\left(\omega^2 R^2\right) \approx \frac{\pi}{50a^6\alpha}, \tag{4.22}$$

which again agrees to our result in (4.13) up to leading order in a.

Similar agreements are obtained for angular momentum and entropy which are obtained to be respectively,

$$L = \int \rho dv \omega R^2 \approx \frac{\pi}{1250a^7\alpha^2}, \tag{4.23}$$

and

$$S = \frac{5\lambda^{1/5}(\rho-\rho_0)^{4/5}V}{4^{4/5}} \approx \frac{\pi}{250a^6\alpha}. \tag{4.24}$$

Although we are never really able to go beyond small a within the validity of fluid dynamics, it is of course true as a purely mathematical fact that a relativistic version of the force balance presented in this subsection may be used to reproduce the exact formulas (to all orders in a) of the thin ring approximation. In the rest of this subsection we describe how that goes.

JHEP03(2009)101

Now for our case of the thin ring the height function is given by (as in (4.10)).

$$h(r) = \sqrt{R_c^2 - (r-R)^2}. \tag{4.25}$$

Using this expression for $h(r)$ into (2.8) and (2.11) we obtain the pressure to be $P = \frac{\sigma(2r-R)}{2rR_c}$. We now plug this back into (2.6) and consider the point $z = 0,\ r = R$. Then if we write the resultant equation in terms of the previously defined parameters α, a we obtain,

$$\tilde{\omega} = \frac{5a^3\alpha}{1-6a^2}, \tag{4.26}$$

which agrees completely to (4.9) up to the leading order in α. Further using the equation of state we can integrate (2.6) to obtain,

$$k = \frac{(\rho-\rho_0)\left(1-v^2\right)^{\frac{5}{2}}}{4\rho_0}, \tag{4.27}$$

k here being the integration constant. We can once again use the equation of state and the expression of pressure obtained above in to this expression for k. Then if we express it in terms of α, a we obtain an exact match with (4.9) up to leading order in α. Once the expressions for $\tilde{\omega}$ and k match up to leading order in α the matching of the expressions for energy, entropy and angular momentum follow immediately.

4.1.3 Thin ring as an inner surface

We now investigate whether a thin ring solution may exist as a inner surface inside a outer surface being a ball or a ring. If the thin ring is to exist as a inner surface the conditions corresponding to (4.2) and (4.3) is changed to,

$$f(a(1-\alpha)) = g(a(1-\alpha)), \tag{4.28}$$

and,

$$f(a(1+\alpha)) = -g(a(1+\alpha)), \tag{4.29}$$

whereas the condition (4.4) remains unchanged (note the all important change in sign).

Note that the constant c that appears in the above equations is in general different from the similar constant that will appear for the outer surface. However Since in our argument bellow we never refer to the outer surface so we continue to use the notation c for this integration constant determined by the surface properties.

As before we can expand (4.28) and (4.29) in terms of the parameter α which is small by the thin ring assumption. Then we get,

$$g'(a) = -\frac{1}{2}f''(a)\alpha a, \tag{4.30}$$

$$g(a) + \frac{1}{2}g''(a)(\alpha a)^2 = -f'(a)\alpha a. \tag{4.31}$$

JHEP03(2009)101

Also as before we have $f(a) = 0$. Solving the above three conditions for $k, \tilde{\omega}$ and c we get the following result,

$$\begin{aligned} k &= \frac{\left(1-a^2\right)^{5/2}\left(\left(84\alpha^2-2\right)a^6+\left(6-75\alpha^2\right)a^4+\left(9\alpha^2-6\right)a^2+2\right)}{12\left(2\alpha^2-1\right)a^6+\left(26-30\alpha^2\right)a^4+\left(9\alpha^2-16\right)a^2+2} \\ \tilde{\omega} &= -\frac{10a^3\left(a^2-1\right)^2\alpha}{12\left(2\alpha^2-1\right)a^6+\left(26-30\alpha^2\right)a^4+\left(9\alpha^2-16\right)a^2+2} \\ c &= \frac{-40\left(6\alpha^2-1\right)a^8+\left(408\alpha^2-94\right)a^6+\left(72-195\alpha^2\right)a^4+2\left(9\alpha^2-11\right)a^2+4}{6\left(12\left(2\alpha^2-1\right)a^6+\left(26-30\alpha^2\right)a^4+\left(9\alpha^2-16\right)a^2+2\right)}. \end{aligned} \tag{4.32}$$

We expand the expressions of k and $\tilde{\omega}$ up to leading order in α to obtain,

$$\begin{aligned} k &= \frac{\left(1-a^2\right)^{7/2}}{1-6a^2} \\ \tilde{\omega} &= \frac{5a^3\alpha}{6a^2-1}. \end{aligned} \tag{4.33}$$

Thus we see that if $a > \frac{1}{\sqrt{6}}$, $\tilde{\omega}$ is positive but k is negative; on the other hand if $a < \frac{1}{\sqrt{6}}$ (especially if $a < \frac{1}{\sqrt{11}}$ where our hydrodynamic approximation is valid) k is positive but $\tilde{\omega}$ is negative. Thus for a given α (or energy) there is no velocity a for which a solution with a thin ring as a inner surface exists.

4.2 The pinched limit of the ring

As we have explained above, the fluid dynamical equations under study in this paper admit two topologically distinct classes of solutions; solid balls and solid tori. The moduli space of ball and ring solutions meet at a point which we call the pinched limit. In this limit the inner radius of the ring goes to zero and the ring closes off into a ball. Approached from the other side, the height function of the ball undergoes an extreme pinch (goes to zero at the center) at this point, opening out into a ring. In this section we study the ring solution in the neighborhood of this topological transition.

In the neighborhood of the pinch, i.e. when $v_i < v \ll 1$,

$$\tilde{h}'(v) = \frac{6\tilde{\omega}v_i + 6(1-k)v_i(v-v_i) + 3(1-k)(v-v_i)^2}{\sqrt{36\tilde{\omega}^2(v-v_i)^2 + 72\tilde{\omega}^2(v-v_i)v_i}}, \tag{4.34}$$

where we have retained terms up to second order in both $v - v_i$ and v_i. It is not difficult to convince for small v_i,

$$\begin{aligned} &\tilde{h}'(v) = \sqrt{\frac{v_i}{2}}\frac{1}{\sqrt{v-v_i}}, && \text{when } (v-v_i) \le 2v_i. \\ &\tilde{h}'(v) = \frac{v_i}{v-v_i}, && \text{when } 2v_i \le (v-v_i) \le \left(\frac{2\tilde{\omega}v_i}{(1-k)}\right)^{\frac{1}{2}} \\ &\tilde{h}'(v) = \frac{(1-k)}{2\tilde{\omega}}(v-v_i), && \text{otherwise.} \end{aligned} \tag{4.35}$$

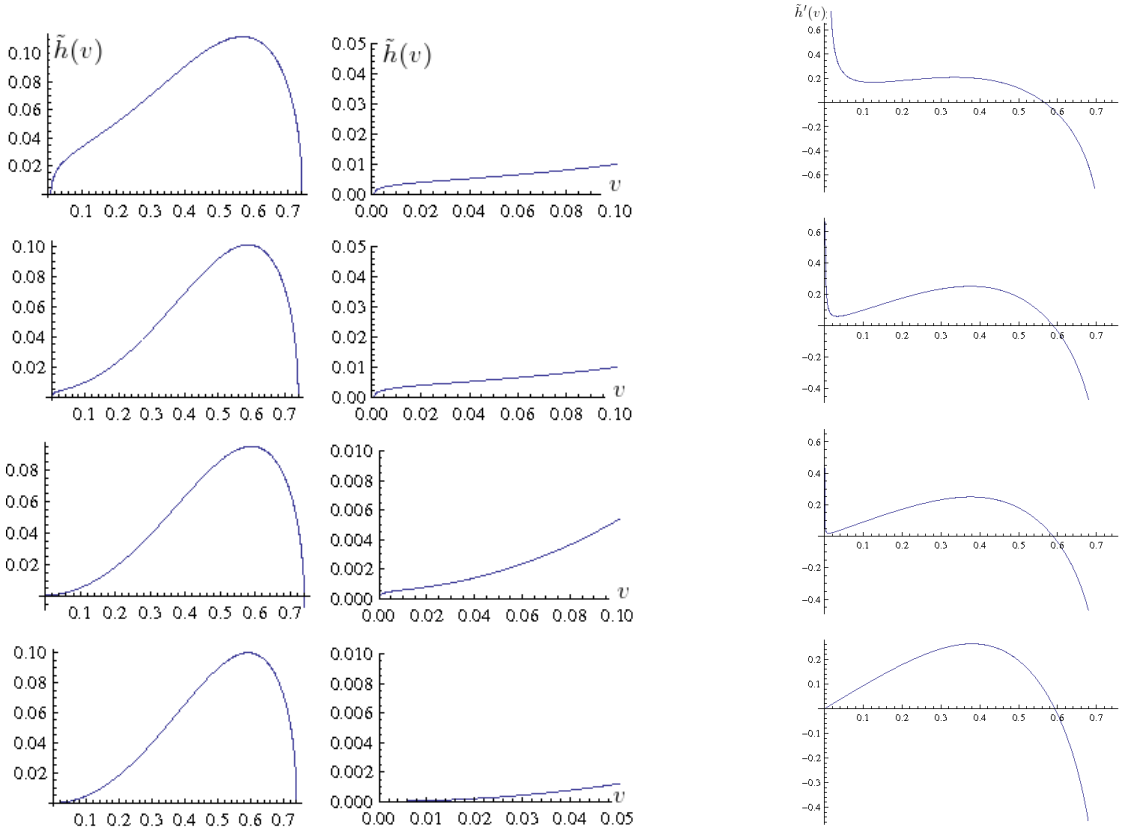

(a) (b)

Figure 4. In (a) we plot $\tilde{h}(v)$ (the plot at the side shows $\tilde{h}(v)$ near $v = v_i$) and in (b) we plot $\tilde{h}'(v)$. All the plots are for $v_o = 0.74$ and the value of v_i are $0.01, 0.001, 0, 0001, 10^{-14}$ as we go from top to bottom.

Note in particular that when v_i is set to zero

$$\tilde{h}(v) = \frac{(1-k)}{4\tilde{\omega}} v^2. \tag{4.36}$$

smoothly matching on the the ball in the limit of extreme pinching. In figure 4 we plot the height function and its derivative at various values of v_i. The transition from the ball to the ring is continuous in configuration space - it is the analogue of a second order phase transition. It would not be difficult to extract the 'critical exponents of this transition from the formulas presented in this paper. However it seems likely that the thin wall approximation used to model the fluid boundary in this paper (see [4, 5] for more details) is inadequate precisely in the strict limit $v_i \to 0$. At least naively we would expect the thin wall approximation to be good only when $v_i \gg \tilde{\omega}$.

JHEP03(2009)101

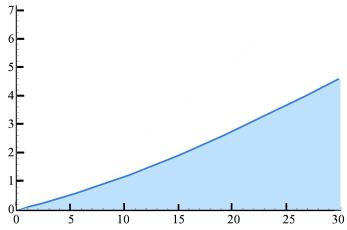

Figure 5. Allowed region of energy (x-axis) and angular momentum (y-axis) space for ordinary ball solution.

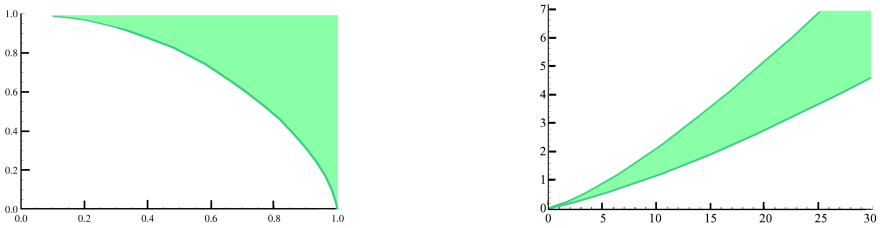

(a) (b)

Figure 6. In (a) we show the allowed region of the v_o (x-axis) and k (y-axis) space where the pinched ball solution exists and in (b) we show the corresponding allowed region of energy (x-axis) and angular momentum (y-axis) space for pinched ball solution.

5 Numerical results

5.1 Thermodynamics of plasma balls

In section 2 we had presented the various solutions along with the expression for their energy, angular momentum and entropy. For the ball-type solution we may take the two independent parameters characterizing the solution to be energy($\tilde{E}$) and angular momentum($\tilde{L}$). Now (2.17) and (2.18) express $\tilde{E}$ and $\tilde{L}$ as functions of two auxiliary parameters k and v_o. Consequently by plotting $\tilde{E}$ and $\tilde{L}$ for any given value of k and v_o, and by varying these parameters over their allowed region, we generate the region of the $\tilde{E}$-$\tilde{L}$ space for which we have ball type solutions. For the ordinary ball we have $k \geq 1$ and $v_o \in [0, 1]$. With these ranges for k[1] and v_o we plot the points generated for $\tilde{E}$ and $\tilde{L}$ on a diagram in figure 5. For the pinched ball solution $k \in [0, 1]$ and so does v_o. However there is also the additional constraint (2.20). Taking this condition into account we plot the allowed values of k and v_o in figure 6(a). Then Using these allowed values we generate the set of allowed points in the $\tilde{E}$-$\tilde{L}$ space and present it in a plot in figure 6(b). As is clear from this figure, ball solutions exist in a certain region of the $\tilde{E}$, $\tilde{L}$ plane, and at no value of energy and angular momentum do we have more than one ball solution.

[1]We considered k up to 7.5 only. With increase in the value of k the region near the energy(x)-axis (i.e. lower values of angular momentum) gets filled; therefore the fact that an upper bound to angular momentum exists at a fixed energy can be asserted with confidence.

JHEP03(2009)101

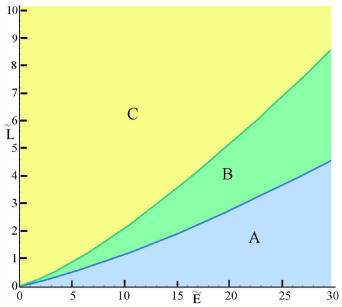

Figure 7. Here we present the $\tilde{E}$ $\tilde{L}$ plane showing regions where the various solutions viz. the ordinary ball, the pinched ball and the ring exists. In region A we have only a single ball solution. In region B we have one ball (either ordinary or pinched) and two ring solutions. In region C we have a single (thin) ring solution.

Using (2.19) we may now compute the entropy of the ball solutions as a function of their energy and angular momentum. In figure 8 (see the left inset) we present a slice of this plot at fixed energy $\tilde{E} = 10$ (for convenience we found a set of values of k and v_o with $\tilde{E} = 10 \pm 0.05$ in order to generate this plot).

5.2 Thermodynamics of plasma rings

We have performed an analysis similar to the one described in the last subsection in order to obtain the region of the $\tilde{E}\tilde{L}$ plane in which ring solutions exist. Once again solutions exist only in a sub space of the $\tilde{E}\tilde{L}$ plane (for any given energy there is a minimum angular momentum above which we have ring type solutions, see figure 7). There are also regions in the $\tilde{E}\tilde{L}$ plane where there exist two distinct ring solutions (we refer to these as thin and thick rings). This region of multiple solutions coincides exactly with the region of the $\tilde{E}\tilde{L}$ plane in which a ball solutions (ordinary or pinched) exists overlaps with that of the ring solution. Putting all this together with the results of the the previous section we see that the $\tilde{E}\tilde{L}$ plane is divided into three distinct regions, A, B, C as shown in figure 7. In region A we have only a single ball solution. In region B we have one ball and two ring solutions. In region C we have a single (thin) ring solution.

In the region B of figure 7, the solution of maximum entropy will dominate the thermodynamics of the system. In order to see how this goes we once again fix $\tilde{E} = 10$ and plot the entropy versus angular momentum of ring solutions in figure 8(see right inset). In figure 8 we also superpose this plot with that of the ball solution to obtain the entropy versus angular momentum plot of all solutions at constant energy. The shape of this final plot is schematically depicted in figure 9(b) We see from this plot that the thick ring solution is always entropically subdominant compared to the ball and the thin ring. As we have explained in the introduction, the ball dominates at smaller angular momenta, while the thin ring is entropically dominant at larger angular momenta.

JHEP03(2009)101

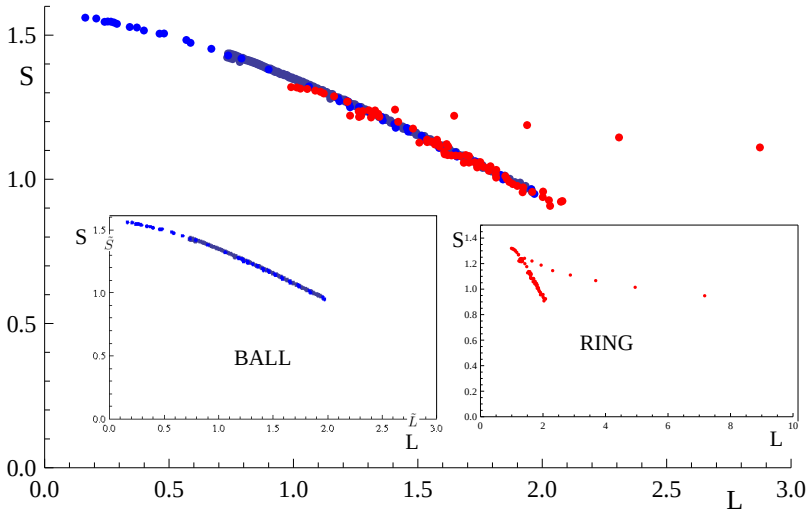

Figure 8. Plot showing $\tilde{S}$(y-axis) vs $\tilde{L}$(x-axis) for all the solutions together.

6 Comparison with the results in flat space

Above we have used the effective fluid dynamical description of the dynamics of the deconfined phase of the field theory dual to gravity on AdS_6 compactified on a Scherk-Schwarz circle to investigate the structure of large rotating black holes and black rings in this gravitational background. In this section we qualitatively compare our results with known results and conjectures about the structure of black holes and black rings in flat six dimensional space.

While rotating Myers Perry black holes have been analytically constructed in flat space six dimensional space, exact black ring solutions have not yet been constructed. Nonetheless Emparan and collaborators [1, 2] have presented physically motivated conjectures for the structure of these solutions (see also [7] for a perturbative construction of a non uniform black string in AdS_6). In this section we will compare the moduli space of solutions obtained in this paper with that conjectured in [1]. We will find some similarities but also other differences. In figure 9(a) we present the relevant part of the conjectured phase diagram (the area of the horizon vs the angular momentum) in asymptotically flat six dimensional space. Here the dark line from A to E through B represents the well known Myers-Perry black holes which is a class of rotating black holes with a spherical (S^4-ordinary ball) horizon topology. The thin line from C to D represents the black ring (with $S^3 \otimes S^1$ topology) and the grey thick line from B to C is the conjectured smooth interpolation from the ordinary ball to the ring type through the 'pinched ball' solutions, with the point C being the point of extreme pinching. It is important to note however that the authors in [1] make it clear that this part of the diagram is a guess.

In figure 9(b) we present qualitatively the phase diagram (Entropy vs angular momentum at constant energy) obtained by us for asymptotically AdS_6 spaces. Here the dark line from A to F represents the rotating black hole with spherical topology which is the analog of Myers-Perry black holes in asymptotically flat space. The two phase diagrams

JHEP03(2009)101

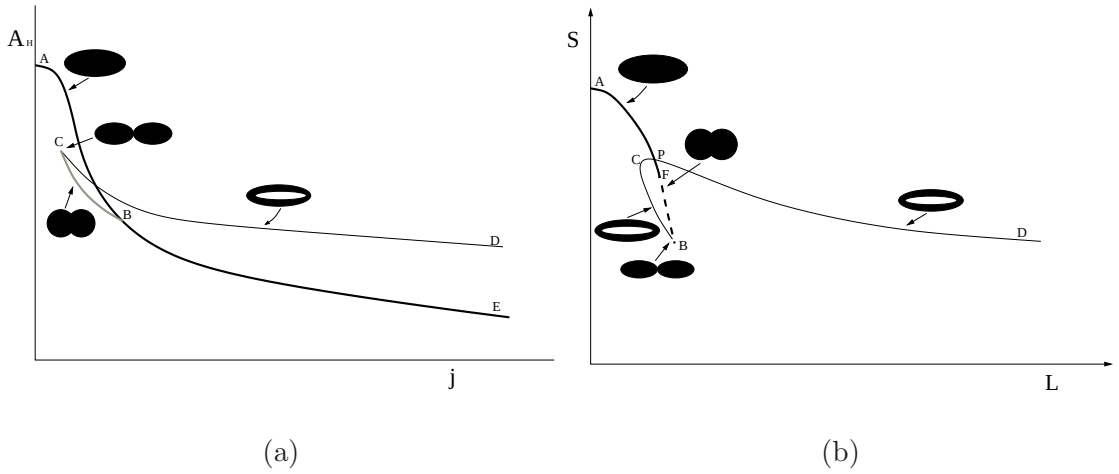

(a) (b)

Figure 9. In (*a*) the area of the horizon has been plotted against angular momentum for black hole topologies in six dimensional asymptotically flat space as in [1] (we present only that part of the phase curve that is relevant for comparison with our result). In (*b*) we summarize our result qualitatively.

have several points of difference. Firstly, at any given energy there exists a Myers-Perry black holes at every value of angular momentum no matter how large. In contrast, at any given energy the ball like fluid solutions determined in this paper exist up to only a finite value of angular momentum. Also in figure 9(b) the segment F to B represents the pinched ball configuration. Note that the ordinary ball smoothly continues into the pinched ball at F. This is unlike the flat space predictions where there is a kink at the point where the ordinary ball continues into a pinched ball (see point B in figure 9(a)).

This important difference feeds into the next point of distinction between figure 9(a) and figure 9(b). As we have explained in our paper, the moduli space of balls ends, at large angular momenta, as an extreme pinched ball. This ball smoothly turns into a thick ring giving rise to the segment BC in figure 9(b) with point B representing the extreme pinched ring. The natural continuation of figure 9(b) to flat space would be to push the point B to infinity as a consequence of which the Myers Perry black holes would 'pinch off' only at infinite angular momentum. This would result in a phase diagram with three solutions at all angular momenta larger than a critical value, with the thick ring always entropically subdominant, and approaching a pinch at infinite angular momenta. In such a scenario the fact that the thin ring is entropically dominant compared to the Myers Perry black holes is similar to that in figure 9(a). However it would still be qualitatively different from figure 9(a). This perhaps suggest that despite similarities there are considerable difference between asymptotically AdS and flat spaces. Such differences between AdS and flat space in five dimensions regarding existence of Saturn type solutions have also been reported in [12]. Alternatively the continuation of figure 9(b) to flat space could be such that the ordinary ball solution is continued from the point F to infinite angular momentum such that the thin ring at large angular momentum is always entropically dominant compared to the ordinary ball. This diagram would be more close to figure 9(a). These diagrams

JHEP03(2009)101

would have a special point where the solution with ball topology would split up into two lines. It would clearly be interesting to have a better understanding of this point.

7 Discussion

At strong coupling the AdS/CFT correspondence identifies the effectively classical large N dynamics of an appropriate boundary theory with gravitational dynamics of the bulk dual. As field theory dynamics reduces to fluid dynamics at long wavelengths, it follows as a prediction of the AdS/CFT correspondence that the appropriate gravitational equations reduce to the equations of boundary fluid dynamics in the long wavelength limit. For the special case that the boundary theory is conformal (and the corresponding bulk solutions asymptote to AdS space) this equivalence has recently been proved, and the corresponding distinguished fluid dynamical system characterized in detail (see [8–11]).

In this paper we have exploited the duality between a 5 dimensional CFT on a Scherk-Schwarz circle and gravity on an asymptotically Scherk-Schwarz AdS_6 space. It follows as a consequence of the results eluded to in the previous paragraph, that long wavelength gravitational dynamics in this bulk background is simply dual to the dimensional reduction of the distinguished equations of fluid dynamics, referred to above, apart from a constant additive piece in the equation of state of the fluid (see [5] for details of this shift). This additive shift implies that the pressure of our fluid (unlike a conformal fluid) goes to zero at a particular finite energy density. This fact permits the existence of qualitatively new solutions of the equations of fluid dynamics in these systems; finite blobs of (perhaps rotating) fluids that are separated from the vacuum by a domain wall (see [5]). In this paper we have investigated the moduli space of static solutions of this nature. These solutions are expected to be dual to localized black holes in the 6 dimensional bulk background.

It may be possible - and would be very interesting - to directly construct the fluid equations that are dual to long distance gravitational dynamics in our background. As we have explained above, all bulk terms in these equations of motion are already known. However the fluid configurations in this paper also have boundaries which play a crucial role in their dynamics. In addition to bulk density and shear waves, such configurations will support fluctuations localized at boundaries; these two types of fluctuations will interact. All of these effects (which may be important in order to study dynamical perturbations of the static solutions investigated in this paper) should directly follow from a thorough investigation of the gravitational equations.

In this paper we have also compared the phase diagram of black holes and black rings in Scherk-Schwarz compactified AdS_6 with that in asymptotically flat space. The most important difference between the two being the absence of black holes with spherical horizon topology in Scherk-Schwarz compactified AdS_6 (the one corresponding to Myers Perry black holes in flat space) beyond a certain angular momentum. The portion of the phase diagram which connects the ball type of solution to the ring is quite speculative in asymptotic flat space. It could be like what we find here for asymptotically Scherk-Schwarz AdS_6 or something else. Any conclusive statement about this region in six dimensional asymptotically flat space demands an intensive gravity calculation.

JHEP03(2009)101

The investigation of fluctuations about our solutions may be interesting for several reasons. It is possible that some of the ring solutions in this paper have Plateau-Rayleigh type instabilities (the instability for a tube of fluid to break up into a chain of droplets) which would be dual to Gregory-Laflamme instabilities of the corresponding black rings (see [6, 13–15] for more details). In more generality, it certainly seems interesting to investigate the dynamical stability of all the solutions studied in this paper.

Finally we would like to draw attention to a curious fact that has emerged from our analysis. Within the fluid dynamical approximation the ring solutions we have studied in this paper have the fluid rotating at a finite universal speed - $\frac{1}{\sqrt{6}}$ - in the extreme thin ring limit (this is also the upper bound on the speed of rotation). It turns out that this extreme limit cannot be reliably studied within the fluid approximation. Nonetheless the qualitative feature of an upper bound to the velocity of rotating rings has also been discovered in flat space [1],[2] though in that case the upper bound velocity is $\frac{1}{\sqrt{3}}$. This makes us suspect that the 'speed limit' uncovered in our analysis is not an artifact of the fluid approximation, but is likely to persist in an exact analysis of black rings in AdS space. This is an issue that calls for further study.

Acknowledgments

The authors would like to thank Shiraz Minwalla for suggesting this problem and providing guidance throughout the project. We would also like to thank S. Lahiri for helpful comments during the project and R. Emparan for insightful comments on the final draft. We also thank all the students of Theory Physics student's room in TIFR especially S. Bhattacharyya, R. Loganayagam, A. Sen, B. Dasgupta, S. Ray and D. Banerjee for help and several useful discussions.

References

[1] R. Emparan, T. Harmark, V. Niarchos, N.A. Obers and M.J. Rodriguez, *The phase structure of higher-dimensional black rings and black holes*, *JHEP* **10** (2007) 110 [arXiv:0708.2181] [SPIRES].

[2] R. Emparan and H.S. Reall, *Black holes in higher dimensions*, *Living Rev. Rel.* **11** (2008) 6 [arXiv:0801.3471] [SPIRES].

[3] R. Emparan and H.S. Reall, *A rotating black ring in five dimensions*, *Phys. Rev. Lett.* **88** (2002) 101101 [hep-th/0110260] [SPIRES].

[4] O. Aharony, S. Minwalla and T. Wiseman, *Plasma-balls in large N gauge theories and localized black holes*, *Class. Quant. Grav.* **23** (2006) 2171 [hep-th/0507219] [SPIRES].

[5] S. Lahiri and S. Minwalla, *Plasmarings as dual black rings*, *JHEP* **05** (2008) 001 [arXiv:0705.3404] [SPIRES].

[6] V. Cardoso and L. Gualtieri, *Equilibrium configurations of fluids and their stability in higher dimensions*, *Class. Quant. Grav.* **23** (2006) 7151 [hep-th/0610004] [SPIRES].

[2] We thank R. Emparan for pointing this out.

JHEP03(2009)101

[7] T. Delsate, *Perturbative non uniform black strings in AdS_6*, *Phys. Lett.* **B 663** (2008) 118 [arXiv:0802.1392] [SPIRES].

[8] S. Bhattacharyya, S. Lahiri, R. Loganayagam and S. Minwalla, *Large rotating AdS black holes from fluid mechanics*, *JHEP* **09** (2008) 054 [arXiv:0708.1770] [SPIRES].

[9] S. Bhattacharyya, V.E. Hubeny, S. Minwalla and M. Rangamani, *Nonlinear fluid dynamics from gravity*, *JHEP* **02** (2008) 045 [arXiv:0712.2456] [SPIRES].

[10] S. Bhattacharyya et al., *Local fluid dynamical entropy from gravity*, *JHEP* **06** (2008) 055 [arXiv:0803.2526] [SPIRES].

[11] S. Bhattacharyya et al., *Forced fluid dynamics from gravity*, *JHEP* **02** (2009) 018 [arXiv:0806.0006] [SPIRES].

[12] J. Evslin and C. Krishnan, *Metastable black saturns*, *JHEP* **09** (2008) 003 [arXiv:0804.4575] [SPIRES].

[13] V. Cardoso and O.J.C. Dias, *Rayleigh-Plateau and Gregory-Laflamme instabilities of black strings*, *Phys. Rev. Lett.* **96** (2006) 181601 [hep-th/0602017] [SPIRES].

[14] V. Cardoso, O.J.C. Dias and L. Gualtieri, *The return of the membrane paradigm? Black holes and strings in the water tap*, *Int. J. Mod. Phys.* **D 17** (2008) 505 [arXiv:0705.2777] [SPIRES].

[15] Y. Brihaye, T. Delsate and E. Radu, *On the stability of AdS black strings*, *Phys. Lett.* **B 662** (2008) 264 [arXiv:0710.4034] [SPIRES].

JHEP03(2009)101